



Cite this: *Phys. Chem. Chem. Phys.*,
2018, 20, 17093

Formation patterns of water clusters in CMK-3 and CMK-5 mesoporous carbons: a computational recognition study

Xuan Peng,^a Surendra Kumar Jain,^b Jayant Kumar Singh,^b Anqi Liu^{cd} and Qibing Jin^a

Grand canonical Monte Carlo simulations are performed to study the adsorption of water in realistic CMK-3 and CMK-5 models at 300 K. The adsorption isotherms are characterized by negligible uptake at lower chemical potentials and complete pore filling once the threshold chemical potential is increased. Results for the isosteric heat of adsorption, radial distribution function (O–O and O–H), hydrogen bond statistics and the cluster size distribution of water molecules are presented. The snapshots of GCMC simulations in CMK-3 and CMK-5 models show that the adsorption happens *via* the formation of water clusters. For the CMK-3 model, it was found that the pore filling occurred *via* the formation of a single water cluster and a few very small clusters. The water cluster size increased with an increase in pore size of the CMK-3 model. For the CMK-5 model, it was found that the adsorption first occurred in the inner porosity (*via* cluster formation). There was no adsorption of water in the outer porosity during the filling of the inner porosity. After the inner porosity was completely filled, the water begins to fill the outer porosity. Snapshots from GCMC simulations of the CMK-5 model clearly show that the water adsorption in the outer porosity occurs *via* the formation and growth of clusters and there was no formation of layers of water in the porosity as seen for nonpolar fluids like nitrogen.

Received 23rd March 2018,
Accepted 30th May 2018

DOI: 10.1039/c8cp01887a

rs.li/pccp

1. Introduction

Porous carbons are largely used in industries for separation, purification and catalysis purposes,^{1–4} owing to their large surface area. The structure and thermodynamic properties of simple fluids, confined in carbon nanopores, have been studied exhaustively.^{5,6} However, the mechanism of the adsorption of water in hydrophobic nanospaces of carbon materials is still largely unclear. Nevertheless, the structure and the thermodynamic properties of water confined in hydrophobic regions are of importance in many scientific disciplines such as chemistry, geology, nanotechnology, and biology. Water adsorption in hydrophobic materials is typically characterized by negligible adsorption at low relative pressures, sudden and complete pore filling by a capillary-condensation mechanism, and large adsorption/desorption hysteresis loops.^{7,8}

Evidence from experiments and molecular simulation show that water adsorption in carbon nanopores follows a different mechanism from that of simple fluids such as nitrogen. For nitrogen, adsorption starts at low pressure and progresses as layers along the pore walls, whereas water adsorption happens around active sites within the material where water can adsorb preferentially, followed by further adsorption through the development of hydrogen bond networks that permeate from these active sites.⁹ Recent work has highlighted the existence of long-lived metastable states of adsorbed water clusters as a cause for hysteresis.^{10,11} Experiments performed by various techniques (adsorption, SAXS, SANS) and theoretical work suggest that the adsorption behavior of water in hydrophobic microporous carbons is controlled by the formation of water clusters of various sizes, which adsorb on existing polar sites (*e.g.*, oxygen) on the carbon walls.^{11,12} Pore filling of a pore of a given width is correlated with a critical water cluster size. Based on this, it seems that the pore condensation of water in the mesopores of CMK is not controlled by the formation of adsorption layers (*i.e.*, multilayer adsorption leading to pore condensation), but by a mechanism similar to water adsorption in purely microporous carbons, which is controlled by the formation of metastable water clusters.

There are a number of reports on the behavior of water adsorption on carbon surfaces or in porous carbons using

^a College of Information Science and Technology, Beijing University of Chemical Technology, Beijing 100029, P. R. China. E-mail: pengxuan@mail.buct.edu.cn

^b Department of Chemical Engineering, Indian Institute of Technology Kanpur, Kanpur, India

^c Center for Safety, Environmental & Energy Conservation Technology of China University of Petroleum, P. R. China

^d CNPC Research Institute of Safety and Environment Technology, P. R. China

computer simulation,^{13–26} but there are few studies on water adsorption in carbon mesopores. It is believed that the water adsorption in hydrophobic mesopores is governed by the growth of clusters. The cluster size in the mesopore is greater than that in the micropore, and it is commensurate with mesopore size. A larger cluster size is required for adsorption of water in the mesopore because the potential energy of a larger cluster is lower than that of a smaller cluster,²⁷ and that is the reason for the adsorption in mesopores occurring over a higher range of pressure because a higher pressure is required to form larger clusters. Essentially, the uptake in pores depends on the number of clusters of certain sizes, and since larger clusters are required for adsorption in larger pores, this is only possible with a higher reduced pressure. This is the reason why adsorption in micropores occurs in a lower reduced pressure while that in mesopores occurs over a higher reduced pressure. Once the clusters on the functional group are sufficiently large, they will enter the pore and the larger the pore, the greater the cluster size required to give a low enough potential for the clusters to remain inside the pore.

Ohba *et al.*²⁸ showed that cluster formation makes the water molecules less hydrophilic because dipole–dipole interaction between water molecules reduces the dipole moment of the cluster as a whole. This reduction of hydrophilicity leads to a higher affinity of the water cluster to the hydrophobic graphitic walls and induces further ordering of the water molecules at filling. The authors have also shown that the clusterization of water molecules in the graphite nanopores transforms the chemical affinity of water molecules from hydrophilic to hydrophobic.²⁸ A single water molecule interacts very weakly with the graphite slit pore. A water molecule can be stabilized by the molecule–molecule interaction in the cluster on cluster formation.

Kaneko *et al.* showed the cluster formation of water molecules using *in situ* X-ray diffraction and *in situ* small-angle X-ray scattering data.^{29–31} Kaneko *et al.* proposed that water vapor can be adsorbed in hydrophobic carbon nanopores free of surface functional groups through cluster formation; namely, once water molecules form the cluster, then the water molecules can be stabilized even in the hydrophobic graphitic nanospace. Thus, water molecules can be accepted by hydrophobic surroundings and the clusters can be accepted by hydrophobic nanoenvironments.

Recently, we have developed realistic molecular models for CMK-3 and CMK-5 carbons.³² We start with a MCM-41 silica pore and perform carbon adsorption (using GCMC simulations), from the vapor phase, in the porosity of the MCM-41 pore. Depending on the thermodynamic conditions, we obtain carbon rods (by complete filling of the porosity of the MCM-41 pore with carbon atoms) or carbon pipes (by wetting the MCM-41 pore with a film of carbon atoms). We arrange the carbon rods in a hexagonal lattice to obtain molecular models for CMK-3 carbons. Similarly, we arrange the carbon pipes in a hexagonal lattice to obtain molecular models for CMK-5 carbons. It is known from experiments that the carbon rods and carbon pipes in CMK-3 and CMK-5 materials are connected

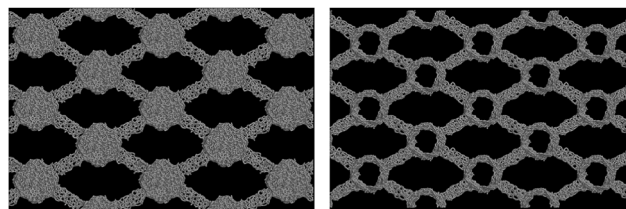


Fig. 1 (left) CMK-3 model and (right) CMK-5 model.

via small interconnections. However, these interconnections are not well characterized from experiments. Thus, we added random interconnections between carbon rods and between carbon pipes to obtain our final CMK-3 and CMK-5 models. More information on the model preparation can be found in our previous report.³² A snapshot of our CMK-3 and CMK-5 models is shown in Fig. 1.

To the best of our knowledge, there has not been any simulation study of water adsorption in CMK-3 and CMK-5 mesoporous carbons.^{32–35} The goal of this work is to understand the mechanism of water adsorption and also the structure of confined water in CMK-3 and CMK-5 mesoporous carbon models. In addition to adsorption isotherms, we also present the isosteric heat of adsorption. Since we are interested in the structure of adsorbed water, we also present the $g_{\text{oo}}(r)$ and $g_{\text{oh}}(r)$ hydrogen bond statistics, cluster size and order parameter (applicable only for the inner porosity of carbon tubes in CMK-5 models). We have not studied the effect of functional groups in this work; however, the effect of functional groups, on the walls of the CMK-3 and CMK-5 models, on water adsorption will be the subject of a forthcoming publication.

2. Simulation methodology

The models of CMK-3 and CMK-5 differ in the inter rod and inter tube distance. This means that the carbon rods and carbon pipes have the same dimension, but the distance between the carbon rods and carbon pipes differ. We used two different inter-rod and inter-pipe distances, *i.e.*, 10A and 14A. Thus, from now on, we will use the nomenclature of CMK3-10A and CMK3-14A for the CMK-3 models with 10A and 14A pore widths and the nomenclature of CMK5-10A and CMK5-14A for the CMK-5 models with 10A and 14A pore widths.

We developed a specific GCMC program to study the adsorption of water at 300 K in our CMK-3 and CMK-5 models. This is because the computational cost of the simulated system is extremely expensive. The number of water molecules at saturated adsorption can reach as high as up to 9000 and 12 000 for CMK3-14A and CMK5-14A, respectively, and the CMK models also contain several thousands of carbon atoms. This shows that our program behaves highly efficiently for simulating such a large size system. As pointed out in our previous work,³⁶ the water models with more than three sites give a more correct orientation that is in better agreement with the one obtained from density functional theory (DFT) calculations. Hence, the TIP4P model for water was used in our work. The carbon

Table 1 Parameters for the TIP4P model of water and CMK adsorbents

Model	σ (Å)	ε (K)	l_1 (Å)	l_2 (Å)	q_1 (e)	q_2 (e)	θ°	φ°
Water	3.154	78.02	0.957	0.15	+0.52	-1.04	104.52	52.26
CMK	3.36	28.0						

Note: l_1 and l_2 are the bond length of OH (namely, the distance between the oxygen atom and the positively charged site q_1) and the distance between the oxygen atom and the negatively charged site q_2 , respectively. Two positively charged sites are located at hydrogen atoms and one negatively charged site is located at q_2 . θ is the angle of \angle HOH and φ is the angle of \angle q_2 OH.

interaction parameters were taken from our previous work.³² The Lorentz–Berthelot rule was used to obtain cross interaction terms. The potential parameters are given in Table 1. In the GCMC method, the chemical potential, box volume and temperature are fixed in the simulation. The GCMC procedure includes particle translation and particle rotation with the usual Metropolis scheme, particle destruction and creation to ensure the chemical potential equilibrium between bulk and pore phases. For all the simulations, the periodic boundary conditions are imposed in three directions. The cut-off radius is 12 Angstrom for the LJ and electrostatic potentials. For each state, a total number of 2×10^9 configurations were generated, where the first 40% of moves were discarded to guarantee the equilibrium and the others were divided into 20 blocks for the ensemble average. We calculated the isosteric heat according to the equation given below,^{33,34}

$$q_{st} \cong kT + \frac{\langle U_{ff} \rangle \langle N \rangle - \langle U_{ff} N \rangle}{\langle N^2 \rangle - \langle N \rangle \langle N \rangle} + \frac{\langle U_{fw} \rangle \langle N \rangle - \langle U_{fw} N \rangle}{\langle N^2 \rangle - \langle N \rangle \langle N \rangle} \quad (1)$$

where the broken brackets denote the ensemble average obtained from simulation, N is the number of adsorbed fluid particles, and U is the configuration energy of the system. In the right-hand side of eqn (1), the second and third terms are the contributions from the fluid–fluid and fluid–wall interactions, respectively.

Since we are interested in the structure of adsorbed water, we calculated the radial distribution function, $g_{oo}(r)$, between the oxygen atoms of water molecules. We also calculated the radial distribution function, $g_{oh}(r)$, between the oxygen and hydrogen atoms. Moreover since, hydrogen bonding (HB) plays a vital role in determining the structural and dynamic properties of water, we calculated the hydrogen bond statistics for the water configurations, obtained from GCMC simulations at different chemical potentials, using the geometrical criteria as described by Swiatla-Wojcik.³⁷ Fig. 2 depicts how we calculate the distances of O–O and O–H between two water molecules separated by one or two hydrogen bonded networks. As previously reported,^{38,39} shortened bond-lengths and red/blue shifts in the IR frequencies are often observed due to the confinement of water. Consequently, it is also interesting to get these hydrogen bond statistics using a full flexible water model. This topic will be addressed in our future work.

It should be noted that in Fig. 2, red circles are oxygen atoms and white circles are hydrogen atoms of water molecules. Thus, A, B, C, D, E, and F depict oxygen atoms and the numbers 1–12

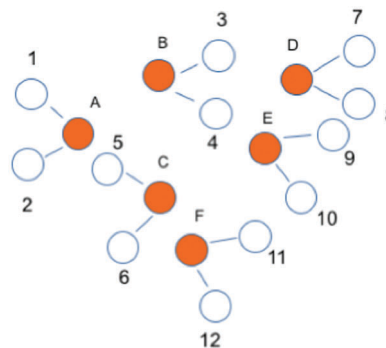


Fig. 2 1st shell and 2nd shell of hydrogen bonded network for water molecule A. The red circles are oxygen atoms and white circles are hydrogen atoms.

depict hydrogen atoms. From Fig. 2, we can see that water molecule A is hydrogen bonded with water molecules B and C. Thus, B and C form the first hydrogen bond shell of water molecule A. Similarly, water molecules D and E form a hydrogen bond with water molecule B and water molecule F forms a hydrogen bond with water molecule C. Thus, the water molecules D, E and F form the 2nd shell of the hydrogen bonded network for water molecule A. Similarly, hydrogen atoms 3, 4, 5, and 6 form the 1st shell of hydrogen bonded atoms for molecule A and hydrogen atoms 7, 8, 9, 10, 11, and 12 form the 2nd shell of hydrogen bonded atoms for molecule A.

We also calculated the cluster size of the adsorbed water molecules from the hydrogen bond information, using a depth first search algorithm. The algorithm is as follows: (a) For each water molecule A, we calculate and store those water molecules B that are hydrogen bonded with A. We do this for all the water molecules. (b) Next, we start with water molecule A and loop over the water molecules that are hydrogen bonded to molecule A. Let us say water molecule B is hydrogen bonded to A. We then loop over the water molecules that are hydrogen bonded to B. Let us call it water molecule C. Similarly, we do this for water molecule C until all the water molecules that are hydrogen bonded together are taken into account. We describe this ensemble of water molecules as belonging to a cluster. (c) In this way, we assign each water molecule as belonging to a cluster. Fig. 3 shows how we determine the clusters of water molecules.

In Fig. 3, there are seven water molecules. The lines connecting the circles are the hydrogen bonds between the two water molecules. Thus, in our cluster algorithm, we count all

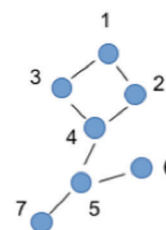


Fig. 3 Cluster of water molecules (the blue circles are water molecules).

the seven water molecules as one water cluster. We do not count water molecules that are cyclic (1–2–3–4) as a separate cluster. We found that if we count the cyclic water molecule clusters, there are very large numbers and sizes of clusters in our CMK models. Also, in counting cyclic water molecules, only two hydrogen bonds of a water molecule are taken into account. Thus, water molecules that have one hydrogen bond will not be calculated as part of a cluster. For example, water molecules 6 and 7 in Fig. 2 will then not be counted as part of a cluster. Thus, we do not consider only cyclic water molecules as a separate cluster.

It should be noted that for the CMK-5 models, we calculate the hydrogen bond statistics and cluster statistics separately for the fluids confined in the inner and outer porosity. We also calculate the orientational order parameter for the water molecules, for the CMK-5 models only, confined in the inner porosity of carbon pipes. The interactions in a hydrogen bonding mixture determine the relative molecular orientations. Hence, the orientation of the molecules near a surface is of interest to us. When the water dipoles are parallel to the pore axis, S equals 1; S equals 0 if the molecules are randomly oriented. It should be noted here that we can calculate the order parameter for the inner porosity of CMK-5 models only, as the inner porosity is similar to the carbon nanotube, but with undulations in the nanopipe walls. The order parameter was calculated according to the equation given below:

$$S = \frac{3\langle \cos^2 \psi \rangle - 1}{2} \quad (2)$$

where ψ is the angle between the water dipole and the pore axis.

3. Results and discussion

3.1. Adsorption isotherms and structure of water in CMK-3 models

In Fig. 4, we present the adsorption isotherms for both the CMK-3 models (CMK3-10A and CMK3-14A). As is well known,

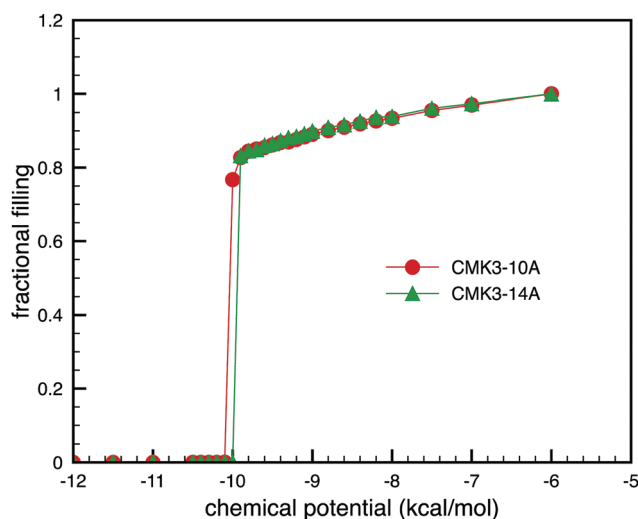


Fig. 4 Adsorption isotherms of water for the CMK3-10A and CMK3-14A models.

at least 46 distinct molecular water models have been developed for reproducing a few specific properties of water.³⁶ These water models show different saturated vapor pressures. For instance, at 300 K, the saturated pressure $P_0 = 0.93$ kPa for the SPCE model and $P_0 = 4.7$ kPa for the TIP4P model, respectively, as compared to the experimental $P_0 = 3.54$ kPa. Furthermore, some researchers¹³ reported the adsorption isotherms of $P/P_0 < 1$, while others²⁴ presented the data of $P/P_0 > 1$. This situation often results in a misleading result when comparing the simulations with the experimental results. Therefore, in this work, we reported the data in chemical potential, instead of relative pressure P/P_0 . The loading is expressed in the unit of fractional filling, which is defined as the ratio of the number of adsorbed molecules normalized by the number of confined molecules corresponding to a completely filled pore with the chemical potential $u = -6.0$ kcal mol⁻¹. As can be seen from the isotherms, there is negligible uptake of water at low chemical potentials and sudden and complete pore filling occurs once a threshold chemical potential is reached. We can see that the sudden jump in adsorption moves to higher chemical potentials as the pore size increases. It should be noted that the only difference between the CMK3-10A and CMK3-14A models is the distance between two carbon rods and the carbon rods are the same for both the models. In Fig. 5, we present the isosteric heat of adsorption for the CMK3-10A model. The isosteric heat follows the same trend for the CMK3-14A model. The total, fluid–fluid and fluid–wall contributions are also shown in Fig. 5. As can be seen, the fluid–wall contribution dominates at low chemical potentials (owing to the presence of defects in the CMK-3 carbon walls). As the chemical potential increases, there is a sudden filling of the pore owing to the sudden formation of water clusters, due to the hydrogen bonding between water molecules. At this point, the fluid–fluid contribution dominates. We want to point out that we did not see the formation of small water clusters at lower chemical potentials that leads to formation of a large cluster *via* merging at increased chemical potentials; rather, we see one full large

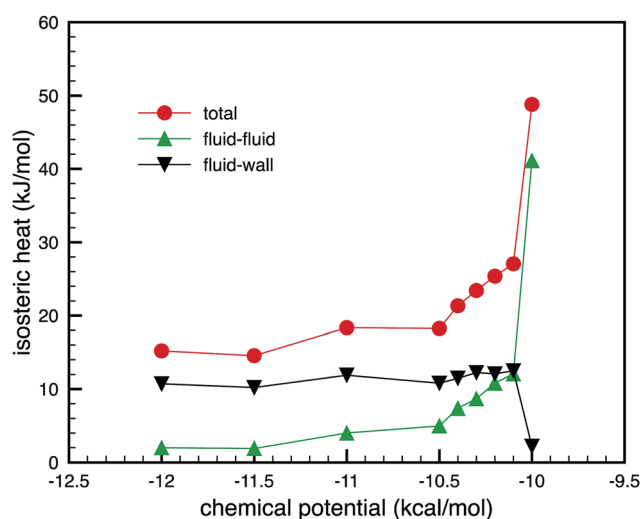


Fig. 5 Isosteric heats of water adsorption for the CMK3-10 model.

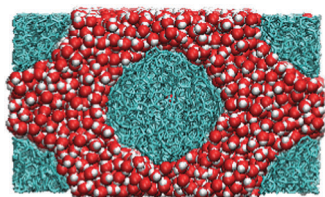


Fig. 6 Snapshot of water molecules in the CMK3-10A model at $u = -9.9$ kcal mol⁻¹.

cluster in the CMK-3 pores. This phenomenon was also observed by Striolo *et al.*¹⁸ in their work on water adsorption in carbon nanotubes. Also, in our CMK-3 models, we do not have any unconnected pores. There are no micropores in the CMK-3 models and the porosity between the carbon rods in the CMK-3 models is totally connected. We show snapshots of the CMK-3 models at pore filling in Fig. 6.

We calculated the O–O distance (between the oxygen atom of a water molecule and oxygen atoms of the water molecules present in the 1st and 2nd hydrogen bonded shells) and the O–H distance (between the oxygen atom of a water molecule and the hydrogen atoms of the water molecules present in the 1st and 2nd hydrogen bonded shells). See the simulation methodology for more details. We show these distances in Tables 2 and 3, for the CMK3-10A model, for two chemical potentials. From Table 2, it can be seen that the O–O and O–H distances decrease as the chemical potential is increased. Specifically, the O–O maximum distance decreases more as the chemical potential is increased, owing to the increase in density of the water molecules. We see this same trend for the O–H distance (Table 3), but to a lesser extent.

To study the structure of water molecules, we present the $g(r)$ for O–O and O–H atoms in our CMK3-10A model in Fig. 7 and 8. From Fig. 7 (for O–O), we can see that there is a peak at ~ 3 Angstrom for all the three chemical potential values. However, we see a shoulder at ~ 4 Angstrom at low chemical potentials and the height of the shoulder decreases and becomes a small minimum at the chemical potential $u = -6.0$ kcal mol⁻¹. Also, there is a small peak at ~ 6 Angstrom for $u = -6.0$ kcal mol⁻¹

Table 2 O–O minimum and maximum distances for the 1st and 2nd hydrogen bonded shells for water molecules for the CMK3-10A model

u (kcal mol ⁻¹)	O–O (max) 1st hydrogen shell	O–O (min) 1st hydrogen shell	O–O (max) 2nd hydrogen shell	O–O (min) 2nd hydrogen shell
-10.0	3.44	2.504	6.44	2.518
-8.0	3.43	2.48	6.39	2.51

Table 3 O–H minimum and maximum distances for the 1st and 2nd hydrogen bonded shells for water molecules for the CMK3-10A model

u (kcal mol ⁻¹)	O–H (max) 1st hydrogen shell	O–H (min) 1st hydrogen shell	O–H (max) 2nd hydrogen shell	O–H (min) 2nd hydrogen shell
-10.0	1.855	1.258	2.537	1.259
-8.0	1.85	1.255	2.528	1.259

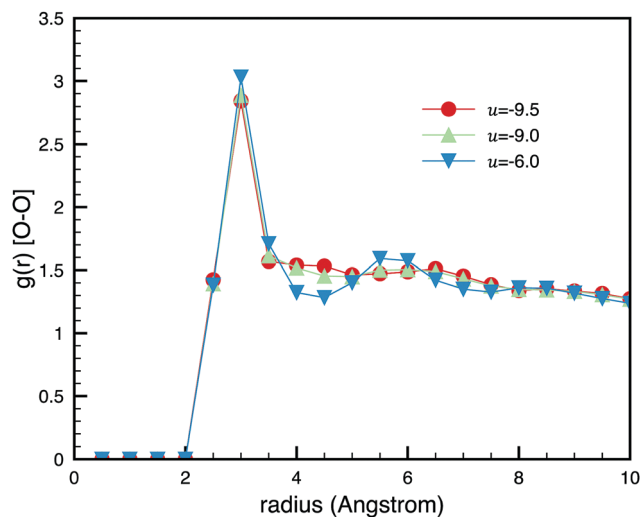


Fig. 7 Pair correlation function for O–O in the CMK3-10A model at different chemical potentials.

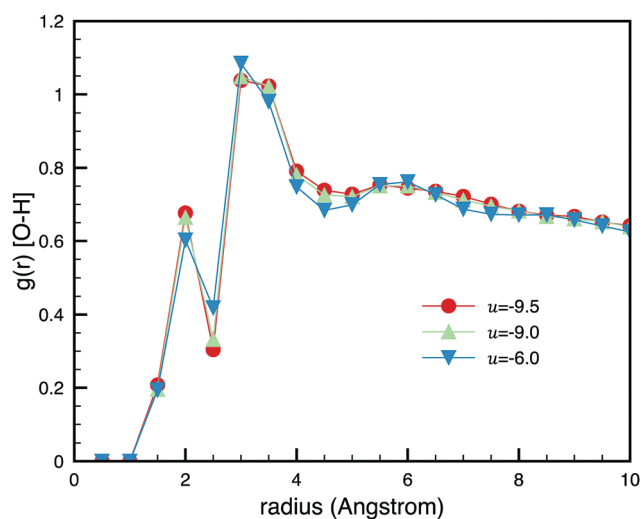


Fig. 8 Pair correlation function for O–H in the CMK3-10A model at different chemical potentials.

that is absent at lower chemical potentials. Thus, the confined water is more structured at high chemical potentials. The shape of $g(r)$ [O–O] is similar for the CMK3-14A model with the first peak slightly smaller than that of the CMK3-10A model. From Fig. 8 (for O–H), we see that the shape of $g(r)$ is almost the same for all the three chemical potentials. At 2 Angstrom, the peak decreases marginally at increasing chemical potential. At ~ 3.2 Angstrom, the peak increases marginally at increasing chemical potential. At ~ 4.2 Angstrom, the height of the curve decreases marginally with increasing chemical potential.

We present the hydrogen bond statistics for the CMK3-14A model in Fig. 9. As can be seen, the fraction of water molecules with 3 and 4 hydrogen bonds dominates in the structure of confined water. We can also see that there is a slight decrease in the fraction of water molecules having HB = 4 at a higher chemical potential $u = -6.0$ kcal mol⁻¹ compared with that at a

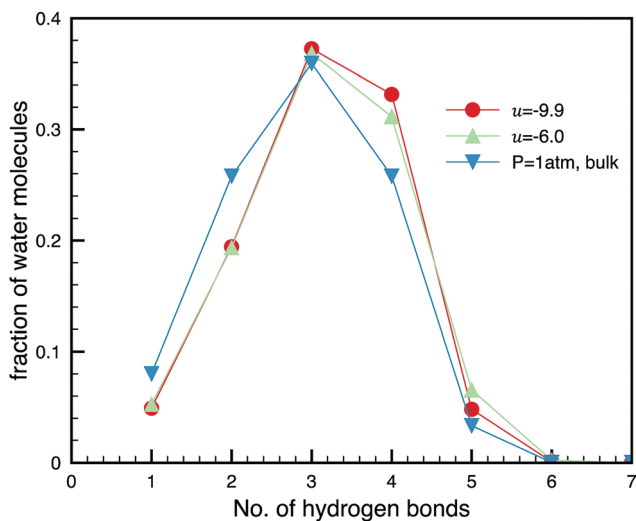


Fig. 9 Hydrogen bond statistics for the CMK3-14A model.

lower chemical potential $u = -9.9 \text{ kcal mol}^{-1}$. There is also a slight increase in the fraction of water molecules having HB = 5 for the higher chemical potential as compared to that at lower chemical potential. We also present the hydrogen bond statistics for bulk water at 1 atm for comparison in Fig. 9. It can be seen that the fraction of water molecules having two hydrogen bonds is large in the bulk as compared to confined water. The fraction of water molecules having three hydrogen bonds is similar in the bulk and in the pore. However, the fraction of water molecules having four hydrogen bonds is lower in the bulk as compared to water confined in the pore. The above observations suggest that water molecules tend to form hydrogen bonds more in confinement as compared to bulk water.

To quantify the water clusters formed *via* hydrogen bonds, we calculated the clusters having different quantities of water molecules (see simulation methodology for the clustering calculation method). The cluster statistics is shown in Table 4 for CMK3-10A. We can see from Table 4 that there are 335 water molecules (for $u = -9.9 \text{ kcal mol}^{-1}$) and 340 water molecules (for $u = -6.0 \text{ kcal mol}^{-1}$) that are present as single entities and are not hydrogen bonded to any other water molecule.

Table 4 Cluster statistics for the CMK3-10A model

Size of cluster	No. of clusters ($u = -9.9 \text{ kcal mol}^{-1}$)	No. of clusters ($u = -6.0 \text{ kcal mol}^{-1}$)
1	335	340
2	78	81
3	44	20
4	12	13
5	10	4
6	6	2
7	6	3
8	3	0
9	3	1
10	3	1
11	3	0
14	0	1
4850	1	0
6267	0	1

This might be due to the distance and angle criteria that we used to calculate hydrogen bonds between two water molecules. Nevertheless, there are water clusters of different sizes (e.g. 2–10) present in the CMK3-10A model. It should be noted that there is a single large cluster present in the CMK3-10A model (4850 for $u = -9.9 \text{ kcal mol}^{-1}$) and (6267 for $u = -6.0 \text{ kcal mol}^{-1}$). This shows that the propensity to form hydrogen bonds increases with increasing chemical potential. Similar results were found for cluster statistics in the CMK3-14A model. Since, the pores of CMK3-14A are bigger, larger clusters were formed in that model.

3.2. Adsorption isotherms and structure of water in CMK-5 models

In Fig. 10, we present the adsorption isotherms for both the CMK-5 models (CMK5-10A and CMK5-14A). As can be seen from the isotherms, there is negligible uptake of water at low chemical potentials. There is a small jump from $u = -9.9 \text{ kcal mol}^{-1}$ to $u = -9.8 \text{ kcal mol}^{-1}$ and also from $u = -9.8 \text{ kcal mol}^{-1}$ to $u = -9.7 \text{ kcal mol}^{-1}$. In the CMK-5 models, there are carbon pipes arranged in a hexagonal lattice (see Fig. 1). Thus, there are two kinds of porosities: inner porosity (inside the tubes) and outer porosity (between the tubes). Thus, the two small jumps relate to the filling of the inner porosity of the central pipe and the filling of the inner pores of the four corner pipes. As the chemical potential is increased, the water clusters are formed in different parts of the pores (as shown in the snapshots below) and at $u = -9.7 \text{ kcal mol}^{-1}$, complete pore filling (porosity between carbon pipes) occurs. It should be noted that the only difference between CMK5-10A and CMK5-14A models is the distance between two carbon pipes and the carbon pipes are the same for both the CMK-5 models. We present the isosteric heat of adsorption for the CMK5-10A model in Fig. 11. As can be seen, the fluid–wall interaction dominates at very low chemical potentials and the fluid–fluid contribution dominates at higher chemical potentials when large water clusters are formed due to hydrogen bonding. By comparing the CMK5-10A isosteric heat

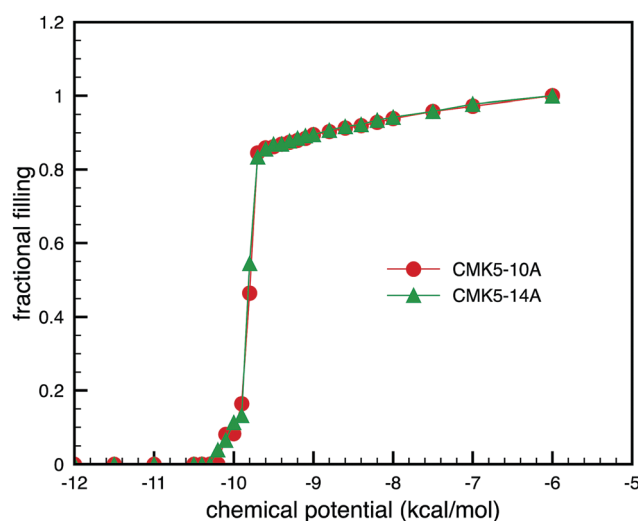


Fig. 10 Adsorption isotherms for the CMK5-10A and CMK5-14A models.

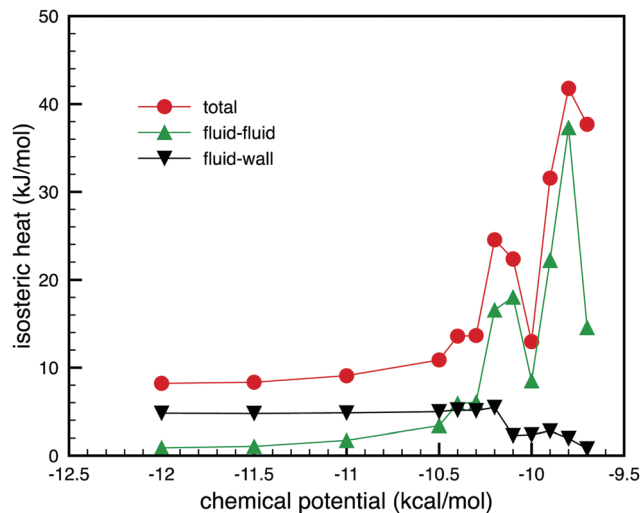


Fig. 11 Isosteric heats of water adsorption for the CMK5-10A model.

with the CMK3-10A isosteric heat, we can see that the fluid-wall contribution is very small in the CMK5-10A model as compared to that of the CMK3-10A model. This is to be expected as there are more water molecules (owing to both the inner and outer porosities) in the CMK5-10A model as compared to the CMK3-10A model (only the outer porosity). Also, it should be noted that in our CMK-5 models, we have unconnected pores (pores in the inner porosity of the central pipe and four corner pipes are not connected) in the inner porosity. The outer porosity, between carbon pipes, forms one large connected pore, which is not connected with the inner porosity.

We show snapshots of the pore filling mechanism in the CMK5-14A model in Fig. 12. From Fig. 12a, we see that at $u = -10.0$ kcal mol⁻¹, the inner porosity of the central pore is completely filled. It should be stressed that there was negligible adsorption at a chemical potential less than $u = -10.0$ kcal mol⁻¹. Moreover, the central inner pipe and the four corner pipes have the same characteristics and thus they exert the same interaction energy towards the water molecules. Initially, very few water molecules get adsorbed in the central pipe and gradually, water clusters grow to fill the complete inner pore. Thus, the pore filling mechanism is through the growth of clusters and not through uniform adsorption. If there were uniform adsorption, the central and four corner pipes would adsorb through layers of water molecules, which was not found in our case. If, in the beginning, water molecules get adsorbed in the corner pipes, then we would have seen the filling of the corner pipes first and then the central pipe, as the central inner pipe and the four corner pipes have the same characteristics. This mechanism was seen for the CMK5-10A model (see Fig. 12f).

In Fig. 12b, it can be seen that the four corner pipes are also filled with water molecules. From Fig. 12c to e, it can be seen that the pores of the CMK5-14A model are filled *via* growth of water clusters and not through layering or uniform adsorption. This is because in Fig. 12c, it can be seen that one portion of the pore is completely filled and there are very few water molecules in the other parts of the pores. So, one part of the pore gets

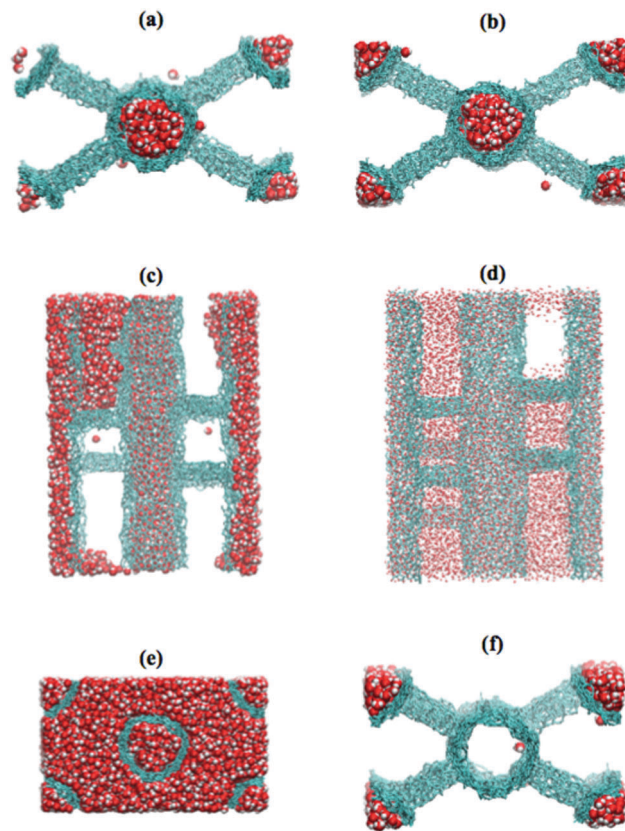


Fig. 12 Snapshot of water molecules in the CMK5-14A model at different chemical potentials, in kcal mol⁻¹. (a) $u = -10.0$; (b) $u = -9.9$; (c) $u = -9.8$; (d) $u = -9.7$; (e) $u = -9.0$; (f) snapshot of water adsorption in the CMK5-10A model at $u = -10.0$. In (d), we show water molecules as bonds to show the CMK5-14A structure also.

filled and then the water molecules fill other parts of the pores *via* the formation of water clusters.

We calculated the O–O distance (between the oxygen atom of a water molecule and the oxygen atoms of the water molecules present in the 1st and 2nd hydrogen bonded shells) and the O–H distance (between the oxygen atom of a water molecule and the hydrogen atoms of the water molecules present in the 1st and 2nd hydrogen bonded shells) (see simulation methodology for more details). We calculated the distances separately for the inner and outer porosities of the CMK5-10A model. We show these distances in Tables 5 and 6, for the CMK5-10A model, for two chemical potentials.

Table 5 O–O minimum and maximum distance for 1st and 2nd hydrogen bonded shells for water molecules for the CMK5-10A model (inner and outer porosity). There are only two water molecules in the outer porosity and thus we have N/A there

Porosity	u (kcal mol ⁻¹)	O–O (max) 1st hydrogen shell	O–O (min) 1st hydrogen shell	O–O (max) 2nd hydrogen shell	O–O (min) 2nd hydrogen shell
Inner	-10.0	3.44	2.48	6.68	2.57
Outer	-10.0	N/A	N/A	N/A	N/A
Inner	-9.7	3.43	2.49	6.31	2.53
Outer	-9.7	3.44	2.42	6.51	2.51

Table 6 O–H minimum and maximum distance for 1st and 2nd hydrogen bonded shells for water molecules for the CMK5-10A model (inner and outer porosity). There are only two water molecules in the outer porosity and thus we have N/A there

Porosity	u (kcal mol ⁻¹)	O–H (max) 1st hydrogen shell	O–H (min) 1st hydrogen shell	O–H (max) 2nd hydrogen shell	O–H (min) 2nd hydrogen shell
Inner	-10.0	1.855	1.255	2.58	1.26
Outer	-10.0	N/A	N/A	N/A	N/A
Inner	-9.7	1.85	1.25	2.51	1.26
Outer	-9.7	1.85	1.24	2.55	1.258

From Table 5, we see that the O–O maximum distance for the 2nd hydrogen bonded shell for the inner porosity decreases with increasing chemical potential. This might be because of the increased density of water molecules upon increasing chemical potential. Again, for the same chemical potential $u = -9.7$ kcal mol⁻¹, the O–O maximum distance for the 2nd hydrogen bonded shell for the outer porosity is larger than that for the inner porosity. This shows that the density of water molecules in the inner porosity is larger than that in the outer porosity. This same trend for the O–H maximum distance for the 2nd hydrogen bonded shell is seen for inner and outer porosity (Table 6).

To study the structure of water molecules, we present the $g(r)$ for O–O and O–H atoms in our CMK5-10A model in Fig. 13 and 14. From Fig. 13 (left), we see that the peak at ~ 3 Angstrom decreases as the chemical potential increases. This is presumably because the total number of water molecules increases with a rise in chemical potential. It should be noted at $u = -10.0$ kcal mol⁻¹, the inner porosity is filled and there are only a few water molecules in the outer porosity. So, the main contribution to $g(r)$, at this chemical potential, is from the inner porosity of the CMK5-10A model. Again, from Fig. 13 (right), we see that the structure of confined water becomes more ordered with increasing chemical potential. There is a hint of a peak

at ~ 6 Angstrom for $u = -6.0$ kcal mol⁻¹. Upon comparing Fig. 13 (right) with the $g(r)$ [O–O] of the CMK3-10A model, we find that the shape of the $g(r)$ is similar, but the peaks are higher for the CMK3-10A model. From Fig. 14 (left), we see that the shapes of the three curves are similar but they are of different heights. The heights of the peaks decrease with the increase in chemical potential, as is seen from the $g(r)$ [O–O] plot in Fig. 13. From Fig. 14 (right), we see the same trend for the CMK3-10A model. However, the peak for the CMK3-10A model is slightly higher than that for the CMK5-10A model.

We present the hydrogen bond statistics in Fig. 15, separately, for water molecules in the inner and outer porosities. As can be seen in Fig. 15 (left), the fraction of water molecules with two hydrogen bonds decrease with the increase in chemical potential. However, the fraction of water molecules with three, four and five hydrogen bonds increases with increasing chemical potential. Interestingly, the fraction of water molecules with four hydrogen bonds decreases for $u = -6.0$ kcal mol⁻¹ as compared to $u = -9.8$ kcal mol⁻¹. From Fig. 15 (right), for the hydrogen bond statistics for the outer porosity, we see that the fraction of water molecules with three and four hydrogen bonds increases with increasing chemical potential. There is a significant increase in the fraction of water molecules with three and four hydrogen bonds from $u = -9.8$ kcal mol⁻¹ to $u = -9.7$ kcal mol⁻¹. However, thereafter, there is not much difference with increasing chemical potential, as can be seen for $u = -6.0$ kcal mol⁻¹. Upon comparing the hydrogen bond statistics for the inner and outer porosities of the CMK5-10A model, we find that the fraction of water molecules with four hydrogen bonds is markedly higher in the case of outer porosity as compared to that of the inner porosity, whereas the fraction of water molecules with two and one hydrogen bonds is higher in the case of inner porosity as compared to that of the outer porosity. The hydrogen bond statistics are similar for the CMK5-10A and CMK5-14A models. The hydrogen bond statistics for CMK5-10A (outer porosity) and CMK3-10A (Fig. 9) are similar. This shows that the overall

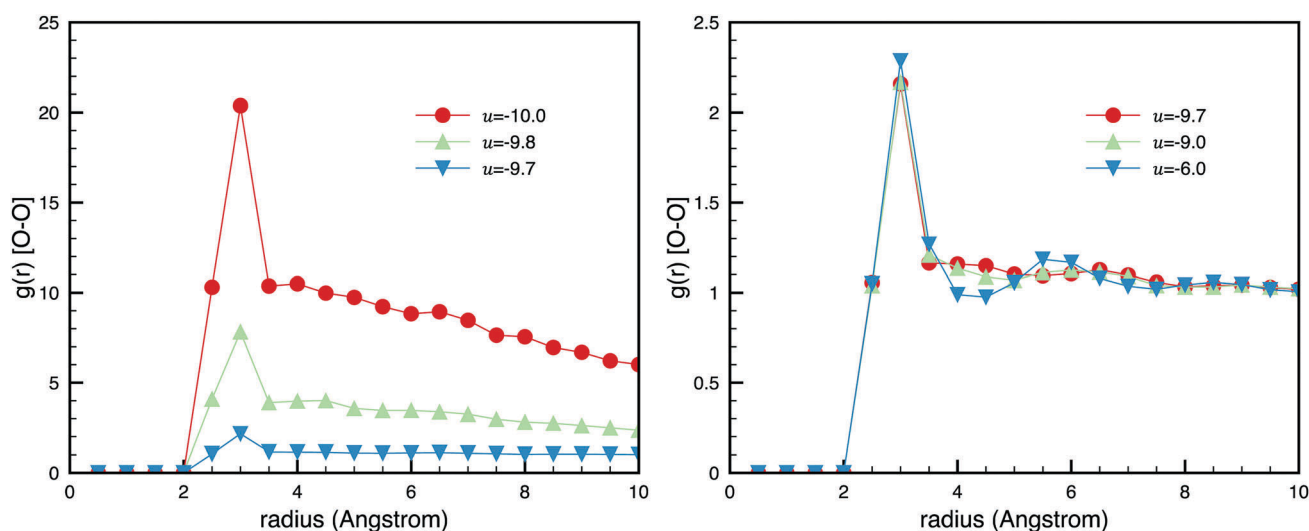


Fig. 13 (left) $g(r)$ [O–O] for three lower chemical potentials and (right) $g(r)$ for higher chemical potentials.

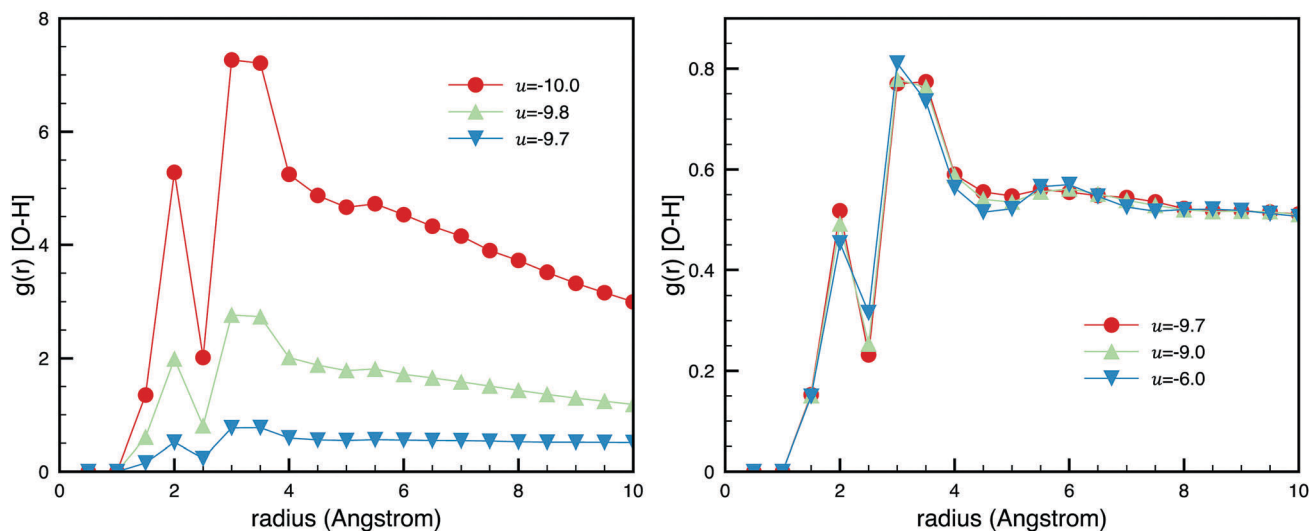


Fig. 14 (left) $g(r)$ [O-H] for three lower chemical potentials and (right) $g(r)$ for higher chemical potentials.

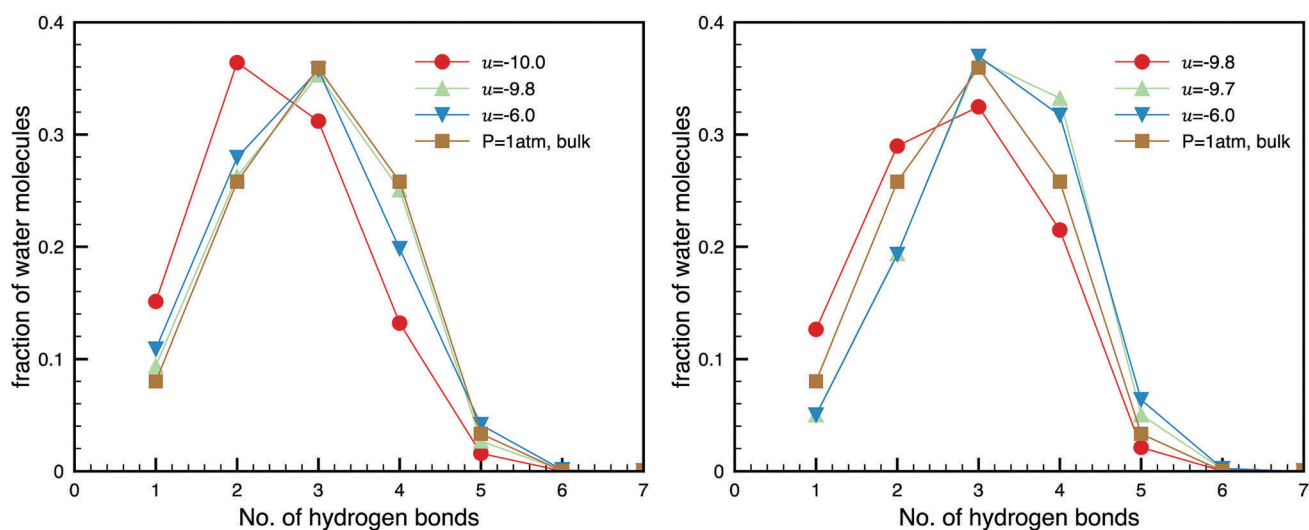


Fig. 15 Hydrogen bond statistics for the CMK5-10A model. (left) For the inner porosity, including the porosity of the central pipe and four truncated pipes and (right) for the outer porosity, the porosity between the carbon nanotubes.

structure of water molecules is similar in both CMK-3 and CMK-5 (outer porosity) models.

We also show the hydrogen bond statistics for bulk water at 1 atm in Fig. 15. Upon comparing the bulk water hydrogen statistics with fluids confined in the inner porosity (Fig. 15, left), it can be seen that the fraction of water molecules having two hydrogen bonds is slightly higher in the pore than in bulk water. The fraction of water molecules having three hydrogen bonds is similar in the bulk and pore. However, the fraction of water molecules having four hydrogen bonds is higher in the bulk as compared to water in the pore. Upon comparing the bulk water hydrogen statistics with water confined in the outer porosity (Fig. 15, right) for higher chemical potentials, it can be seen that the fraction of water molecules having two hydrogen bonds is large in the bulk as compared to confined water. The fraction of water molecules having three hydrogen bonds is

similar in the bulk and in the pore. However, the fraction of water molecules having four hydrogen bonds is lower in the bulk as compared to water confined in the pore. This observation of the outer porosity, of the CMK-5 models, is similar to that found for the CMK-3 models.

To quantify the water clusters formed *via* hydrogen bonds, we calculated the clusters having different quantities of water molecules (see simulation methodology for the clustering calculation method) for the CMK5-10A model. We found that the inner porosity has many small to medium clusters. The largest cluster found consisted of 684 water molecules. The cluster statistics for the outer porosity is shown in Table 7 for CMK5-10A. From Table 7, we found that there are many water molecules that are not part of any hydrogen bonded network. This was also found for the CMK3-10A model. Nevertheless, there are water clusters of different sizes (*e.g.* 2–10) present in

Table 7 Cluster statistics for the CMK5-10A model

Size of cluster	No. of clusters ($u = -9.7$ kcal mol ⁻¹)	No. of clusters ($u = -6.0$ kcal mol ⁻¹)
1	370	308
2	101	83
3	41	22
4	20	10
5	7	5
6	9	1
7	2	4
8	6	2
9	1	2
10	0	2
12	0	1
14	0	1
19	1	0
20	0	1
39	1	0
5927	1	0
7356	0	1

the CMK5-10A model. It should be noted that there is a single large cluster present in the CMK5-10A model at the chemical potential $u = -9.7$ kcal mol⁻¹ (5927) and $u = -6.0$ kcal mol⁻¹ (7356). This shows that the propensity to form hydrogen bonds increases with increasing chemical potential. Similar results were found for cluster statistics in the CMK5-14A model. Since the outer porosity of the CMK5-14A model is greater than that of the CMK5-10A model, larger clusters were formed in the CMK5-14A model.

We also show the radial dependence of the orientational order parameter for water molecules confined in the inner porosity of the CMK5-10A model (at $u = -6.0$ kcal mol⁻¹) in Fig. 16. As can be seen from Fig. 16, the dipole moments of water molecules are randomly oriented ($S(r) \sim 0$), and these water molecules are farther away from the carbon nanopipe wall and near to the center of the inner pore. At the distance of ~ 9 Angstrom from the center of the inner pore, we see that the

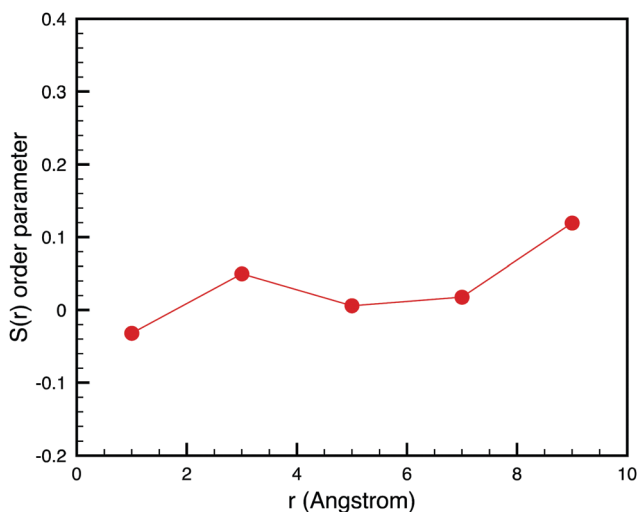


Fig. 16 Order parameter, $S(r)$, along the pore radii for water molecules confined in the inner porosity, of the central carbon nanopipe, of the CMK5-10A model, at $u = -6.0$ kcal mol⁻¹.

order parameter, $S(r)$, takes a value of 0.11, which suggest that dipoles of some water molecules are oriented along the pore axis. There are 131 water molecules at a distance of ~ 9 Angstrom from the center of the nanopipe at $u = -6.0$ kcal mol⁻¹. In a study of water adsorption in carbon nanotubes, Striolo *et al.*¹⁸ found that the water molecules near the carbon nanotube wall have their dipoles oriented along the pore axis and randomly oriented for the water molecules farther away from the nanotube wall. We want to emphasize the point that our carbon nanopipes (of the CMK-5 models) have a surface roughness and appreciable corrugation as opposed to carbon nanotubes, which have smooth walls. This is the reason that we do not see many water molecules with dipoles oriented along the pore axis direction.

4. Conclusions

Grand canonical Monte Carlo simulations were used to study water adsorption in realistic CMK-3 and CMK-5 mesoporous carbon models. The 300 K adsorption isotherms show that the water uptake is negligible at low chemical potentials; the pores suddenly and completely fill once a threshold chemical potential is reached. The pore filling for the CMK-3 model occurred *via* formation of a large stable cluster as there is a single connected pore (porosity between carbon rods). The pore filling for CMK-5 occurred by a two-step mechanism. First, the inner porosity (of carbon pipes) is filled with water *via* the formation of the cluster and then the outer porosity is filled. The inner and outer porosities of the CMK-5 models are unconnected. We found that there was no adsorption of water molecules in the outer porosity during the filling of the inner porosity, which was in sharp contrast with the results obtained for argon adsorption in the CMK-5 models. It was found that, for the outer porosity, water adsorption occurs at one part of the pore, *via* the formation of a stable cluster, and the adsorption progresses to other parts of the pore *via* the growth of the cluster. Our results suggest that the underlying pore-filling mechanism of water into hydrophobic carbon mesopores deviates from conventional capillary condensation (for wetting adsorbates such as nitrogen and argon) but is consistent with the assumption of a clustering mechanism (which had been identified as the underlying mechanism for water adsorption into microporous carbons).

Conflicts of interest

There are no conflicts to declare.

Acknowledgements

X. P. is grateful to the “CHEMCLOUDCOMPUTING” of BUCT for computational support and the National Natural Science Foundation of China (No. 21676006) for financial support. J. K. S. is grateful to the Ministry of Earth Science, Government of India for financial support (MOES/16/16/2013-RDEAS).

References

- 1 E. N. Rudisill, J. J. Hacskeylo and M. D. LeVan, Coadsorption of hydrocarbons and water on BPL activated carbon, *Ind. Eng. Chem. Res.*, 1992, **31**, 1122–1130.
- 2 S. Sircar, T. C. Golden and M. B. Rao, Activated carbon for gas separation and storage, *Carbon N. Y.*, 1996, **34**, 1–12.
- 3 N. A. Seaton, S. P. Friedman, J. M. D. MacElroy and B. J. Murphy, The Molecular Sieving Mechanism in Carbon Molecular Sieves: A Molecular Dynamics and Critical Path Analysis, *Langmuir*, 1997, **13**, 1199–1204.
- 4 X. Peng, W. Wang, R. Xue and Z. Shen, Adsorption separation of CH₄/CO₂ on mesocarbon microbeads: Experiment and modeling, *AIChE J.*, 2006, **52**, 994–1003.
- 5 S. Jiang, C. L. Rhykerd and K. E. Gubbins, Layering, freezing transitions, capillary condensation and diffusion of methane in slit carbon pores, *Mol. Phys.*, 1993, **79**, 373–391.
- 6 R. F. Cracknell, D. Nicholson and N. Quirke, A grand canonical Monte Carlo study of Lennard-Jones mixtures in slit shaped pores, *Mol. Phys.*, 1993, **80**, 885–897.
- 7 K. S. W. Gregg and S. J. S. Sing, *Adsorption, Surface Area and Porosity*, Academic Press, London, 2nd edn, 1982.
- 8 J. K. Brennan, T. J. Badosz, K. T. Thomson and K. E. Gubbins, Water in porous carbons, *Colloids Surf., A*, 2001, **187–188**, 539–568.
- 9 J.-C. Liu and P. A. Monson, Monte Carlo Simulation Study of Water Adsorption in Activated Carbon, *Ind. Eng. Chem. Res.*, 2006, **45**, 5649–5656.
- 10 T. Ohba and K. Kaneko, Kinetically Forbidden Transformations of Water Molecular Assemblies in Hydrophobic Micropores, *Langmuir*, 2011, **27**, 7609–7613.
- 11 T. Horikawa, T. Sekida, J. Hayashi, M. Katoh and D. D. Do, A new adsorption–desorption model for water adsorption in porous carbons, *Carbon N. Y.*, 2011, **49**, 416–424.
- 12 T. Kimura, H. Kanoh, T. Kanda, T. Ohkubo, Y. Hattori, Y. Higaonna, R. Denoyel and K. Kaneko, Cluster-associated filling of water in hydrophobic carbon micropores, *J. Phys. Chem. B*, 2004, **108**, 14043–14048.
- 13 T. X. Nguyen and S. K. Bhatia, How Water Adsorbs in Hydrophobic Nanospaces, *J. Phys. Chem. C*, 2011, **115**, 16606–16612.
- 14 T. X. Nguyen and S. K. Bhatia, Some Anomalies in the Self-Diffusion of Water in Disordered Carbons, *J. Phys. Chem. C*, 2012, **116**, 3667–3676.
- 15 M. Jorge, C. Schumacher and N. A. Seaton, Simulation Study of the Effect of the Chemical Heterogeneity of Activated Carbon on Water Adsorption, *Langmuir*, 2002, **18**, 9296–9306.
- 16 A. Striolo, A. A. Chialvo, P. T. Cummings and K. E. Gubbins, Water Adsorption in Carbon-Slit Nanopores, *Langmuir*, 2003, **19**, 8583–8591.
- 17 A. Striolo, A. A. Chialvo, P. T. Cummings and K. E. Gubbins, Simulated water adsorption in chemically heterogeneous carbon nanotubes, *J. Chem. Phys.*, 2006, **124**, 74710.
- 18 A. Striolo, A. A. Chialvo, K. E. Gubbins and P. T. Cummings, Water in carbon nanotubes: Adsorption isotherms and thermodynamic properties from molecular simulation, *J. Chem. Phys.*, 2005, **122**, 234712.
- 19 G. R. Birkett and D. D. Do, Simulation Study of Water Adsorption on Carbon Black: The Effect of Graphite Water Interaction Strength, *J. Phys. Chem. C*, 2007, **111**, 5735–5742.
- 20 S. Picaud, B. Collignon, P. N. M. Hoang and J.-C. Rayez, Adsorption of water molecules on partially oxidized graphite surfaces: a molecular dynamics study of the competition between OH and COOH sites, *Phys. Chem. Chem. Phys.*, 2008, **10**, 6998–7009.
- 21 T. Ohba and K. Kaneko, Surface Oxygen-Dependent Water Cluster Growth in Carbon Nanospaces with GCMC Simulation-Aided in Situ SAXS, *J. Phys. Chem. C*, 2007, **111**, 6207–6214.
- 22 T. Ohba and K. Kaneko, Cluster-associated filling of water molecules in slit-shaped graphitic nanopores, *Mol. Phys.*, 2007, **105**, 139–145.
- 23 J.-C. Liu and P. A. Monson, Does Water Condense in Carbon Pores?, *Langmuir*, 2005, **21**, 10219–10225.
- 24 A. Wongkoblap and D. D. Do, Adsorption of Water in Finite Length Carbon Slit Pore: Comparison between Computer Simulation and Experiment, *J. Phys. Chem. B*, 2007, **111**, 13949–13956.
- 25 A. Wongkoblap and D. D. Do, The effects of curvature and surface heterogeneity on the adsorption of water in finite length carbon nanopores: a computer simulation study, *Mol. Phys.*, 2008, **106**, 627–641.
- 26 A. Wongkoblap and D. D. Do, Adsorption of polar and nonpolar fluids in finite-length carbon slit pore: a monte carlo simulation study, *Chem. Eng. Commun.*, 2008, **195**, 1382–1395.
- 27 K. Kaneko, T. Itoh and T. Fujimori, Collective Interactions of Molecules with an Interfacial Solid, *Chem. Lett.*, 2012, **41**, 466–475.
- 28 T. Ohba, H. Kanoh and K. Kaneko, Affinity Transformation from Hydrophilicity to Hydrophobicity of Water Molecules on the Basis of Adsorption of Water in Graphitic Nanopores, *J. Am. Chem. Soc.*, 2004, **126**, 1560–1562.
- 29 T. Iiyama, M. Ruike and K. Kaneko, Structural mechanism of water adsorption in hydrophobic micropores from in situ small angle X-ray scattering, *Chem. Phys. Lett.*, 2000, **331**, 359–364.
- 30 T. Iiyama, K. Nishikawa, T. Otowa and K. Kaneko, An Ordered Water Molecular Assembly Structure in a Slit-Shaped Carbon Nanospace, *J. Phys. Chem.*, 1995, **99**, 10075–10076.
- 31 T. Iiyama, K. Nishikawa, T. Suzuki and K. Kaneko, Study of the structure of a water molecular assembly in a hydrophobic nanospace at low temperature with in situ X-ray diffraction, *Chem. Phys. Lett.*, 1997, **274**, 152–158.
- 32 S. K. Jain, R. J.-M. Pellenq, K. E. Gubbins and X. Peng, Molecular Modeling and Adsorption Properties of Ordered Silica-Templated CMK Mesoporous Carbons, *Langmuir*, 2017, **33**, 2109–2121.
- 33 X. Peng, D. Cao and W. Wang, Computational Characterization of Hexagonally Ordered Carbon Nanopipes CMK-5 and Structural Optimization for H-2 Storage, *Langmuir*, 2009, **25**, 10863–10872.

- 34 X. Peng, D. Cao and W. Wang, Adsorption and separation of CH₄/CO₂/N₂/H₂/CO mixtures in hexagonally ordered carbon nanopipes CMK-5, *Chem. Eng. Sci.*, 2011, **66**, 2266–2276.
- 35 X. Peng and S. K. Jain, Atomic simulation of Xe and Kr separation in silica-templated amorphous mesoporous carbons CMK-3 and CMK-5, *Mol. Simul.*, 2017, **43**, 1546–1555.
- 36 X. Peng, L.-C. Lin, W. Sun and B. Smit, Water Adsorption in Metal-Organic Frameworks with Open-Metal Sites, *AIChE J.*, 2015, **61**, 677–687.
- 37 D. Swiatla-Wojcik, Evaluation of the criteria of hydrogen bonding in highly associated liquids, *Chem. Phys.*, 2007, **342**, 260–266.
- 38 O. Shameema, C. N. Ramachandran and N. Sathyamurthy, Blue Shift in X–H Stretching Frequency of Molecules Due to Confinement, *J. Phys. Chem. A*, 2006, **110**, 2–4.
- 39 P. J. Mohan, A. Datta, S. S. Mallajosyula and S. K. Pati, Structures of Nucleobases Trapped within Au Triangles and Its Effects on Hydrogen Bonding in Base Pairs of DNA, *J. Phys. Chem. B*, 2006, **110**, 18661–18664.